Article

Investigation of Parallel and Orthogonal MIMO Antennas with 2-Notched Structure for UWB Application

Liang Wang, Ziwei Li, and Hongxing Zheng *

[1] School of Electronics and Information Engineering, Hebei University of Technology, Tianjin 300401, China; 202131903076@stu.hebut.edu.cn (L.W.); 202131903076@stu.hebut.edu.cn (Z.L.)

* Correspondence: Hongxing Zheng, hxzheng@hebut.edu.cn; Tel.: +86-22-60438244 (optional; include country code; if there are multiple corresponding authors, add author initials)

Abstract: In order to solve the interference of narrowband in the ultra-wideband (UWB) system, a high isolation of multiple-input multiple-output (MIMO) antenna is investigated in this paper. The MIMO antenna consists of 2 or 4 UWB elements; and each UWB antenna element is a monopole reconstructed with 2-notched slots, a U-shaped and inverted U-shaped slots etched on the monopole patch to achieve notch characteristics in WIMAX and ITU bands. The property of a 2-element MIMO antenna is analyzed firstly, which is put into a same substrate in parallel. Two rectangular branches (RB) are located in the middle to reduce the coupling. Then a 4-element MIMO antenna is studied to meet big size space and more application scenarios. Each element is placed orthogonally on the same substrate; and the isolation is implemented by a cross-shaped branch located in the middle of elements. Both MIMO antenna samples have been tested to verify the design. Measured results show that the working bandwidth is 2.45-14.88 GHz and 2.14-14.95 GHz, the isolation is greater than 17 dB and 20 dB, the peak gain is 5.7 dB and 5.9 dB, the maximum radiation efficiency can reach 96% and 95%, the envelope correlation coefficient is less than 0.02 and 0.05 for the 2- and 4-element UWB MIMO antenna, respectively. They both are with very good omnidirectional characteristic with notched bands such as the WIMAX and ITU, and meet the requirements of the UWB application in most cases.

Keywords: coplanar waveguide; double band-notched; MIMO antenna; UWB antenna; isolation; orthogonal elements

1. Introduction

Since the application of ultra-wideband (UWB) frequency was proposed, it has become the focus of many engineers of wireless communication technology. Due to the higher transmission rate and lower power consumption, the UWB technology has been widely used in the fields of ground-penetrating radar [1], [2], wireless sensor [3], precise positioning [4], and biomedical engineering [5], [6], etc. However, the presence of many narrowband communication systems creates some interferes to the UWB system because those frequency bands are also included in the operating band of the UWB system. For example, the Worldwide Interoperability for Microwave Access (WiMAX, 3.3-3.7 GHz) and International Telecommunication Union band (ITU, 8.01-8.5 GHz) etc. At present, the simplest method to filter the interference of the narrowband signal is designing an antenna with band-notched property. To achieve the notch property, antenna is etched slots [7], [8], added defected ground structures [9] and attached parasitic elements [10], [11]. The advantages of those methods were with simple structure, easy design, and the size of antenna is not increased, which are conducive to the miniaturization and large-scale integration of the antenna.

The disadvantage of UWB system is difficult to achieve long-distance transmission under the condition of limited power, and the channel is with rich frequency components, belonging to the high-frequency selective fading channel. If the signal length is smaller than the path delay, very

 doi:10.20944/preprints202306.0836.v1

serious inter-signal interference occurred. Thus, the signal transmission efficiency and quality for the UWB system are degraded. In order to solve these problems, a multiple-input multiple-output (MIMO) technology is introduced, which can increase the channel capacity and improve the transmission quality by using multiple antenna elements in the transmitter and receiver [12]. The MIMO combined with UWB technologies can increase the signal transmission distance without extra energy consumption, and decrease the disadvantage caused by the multipath fading. In many practical scenarios, the MIMO antennas in UWB application system are required to be as small as possible to meet integration of system. However, the strong coupling might be generated between antenna elements within too small distance. It is necessary for us to increase the isolation between them. To decrease the coupling, some methods have been introduced, such as conductor branches [13], etching slots [14], loading neutralization line [15], [16], and other reasonable layout of antenna elements [17]-[22].

In this approach, we use the UWB antenna, but the interferences of the WIMAX and ITU bands must be filtered. Therefore, a UWB antenna with 2-notched characteristics is investigated. To meet the system with higher quality transmission, the MIMO antenna technique using the proposed UWB antenna elements is also studied. First, the characteristics of suppressing WIMAX and ITU bands interference on UWB system is considered. We etch two U-shaped slots on a monopole patch, with traditional curved edge trapezoidal structure. Adjusting its size, we obtained the bandwidth from 2.1-14.9 GHz of the antenna with stopbands of 3.3-3.7 GHz and 8.01-8.5 GHz. This design meets for the IEEE 802.16 standard.

Then, use the designed antenna element we consider the MIMO application. Two-element UWB antenna above is put in parallel style. Two rectangular patches are added between them, which can archive 17 dB of isolation. The notched bands have not been affected. This style is only used in the one-input one-output case. In order to adapt to the real MIMO application scenarios, a four-element UWB antenna above is designed again, which is put into orthogonal style. Then a cross-shaped rectangular patch is used as an isolation component. The isolation can reach 20 dB between each antenna element. The notched bands, WIMAX and ITU have not been changed. The simulation and measurement results show that proposed two MIMO antennas have a good performance of compact in size. Specially, the isolation of 2- and 4-element antennas is archived more than 17 dB and 20dB, respectively, compared to the similar design. It can be widely used in various wireless communication system.

The rest of content is organized as follows. A 2-element and more compact 4-element orthogonal MIMO antenna are proposed with 2-notched characteristics at WIMAX and ITU bands. The total antenna structure design with its geometric specifications is introduced Section II. The notch and decoupling design of the two antennas are simulated and the corresponding parameters and principles are analyzed in Section III, where the scattering matrix, radiation pattern, and the current distribution is simulated. Fabricated sample is measured in Section IV, and results from simulation and experiment have been discussed. Finally, conclusions are drawn in last Section.

2. Two MIMO Antenna structure design

A 2-notched antenna element design is based on a classical UWB monopole, where two identical elements form a MIMO antenna. Each element is fed by the coplanar waveguide (CPW), and two U-shaped slots are etched on the radiating patch to filter the interferences of the WIMAX and ITU bands. Our investigation will be built around this UWB antenna element.

One MIMO antenna consists of two-element and the other of four-element as shown in Figure 1(a) and (b), respectively. The two MIMO antennas have the same antenna element, which adopts microstrip monopole antenna structure, including a semicircular radiation patch, two inverted trapezoidal radiation patch, feeder and ground plane. The width of the feeder is W_m to meet the impedance matching of 50 Ω. In this paper, U-shaped slots are etched on the radiation patch of the antenna element to realize the notch of WIMAX band, and inverted U-shaped slots are etched on the feeder of the antenna element to obtain the notch of ITU band. To obtain the notch property, the most important thing to calculate is the total length of the etched slot. The total length of the slot can be estimated by formula (1) and (2):

Preprints (www.preprints.org) | NOT PEER-REVIEWED | Posted: 12 June 2023 doi:10.20944/preprints202306.0836.v1

$$f_n = \frac{c}{2L\sqrt{\varepsilon_e}} \tag{1}$$

$$\varepsilon_e = \frac{\varepsilon_r + 1}{2} \tag{2}$$

Where, f_n is the center frequency of notch; c is the speed of light; L is the length of the slot; ε_e is the equivalent permittivity; ε_r is the dielectric constant of the dielectric substrate. According to formula (1) and (2), the length of the U-shaped slot is about 26mm when the center frequency is 3.5GHz, and the length of the inverted U-shaped slot is about 11mm when the center frequency is 8.3GHz. After simulating and optimizing with the electromagnetic simulation software High Frequency Structure Simulator (HFSS), it is found that when the length of the U-shaped slot is 25.8 mm and the length of the inverted U-shaped slot is 11.8 mm, the stopband characteristics are the best, which can completely cover the WIMAX and ITU bands, respectively.

The antenna elements of the two-element MIMO antenna are placed symmetrically, and two RB are loaded between the antenna elements. The two RB can generate two new current paths, reduce the coupling current between the ports, and improve the isolation between the antenna elements. The four antenna elements of the four-element MIMO antenna are placed orthogonal to each other, and the antenna elements have different polarization modes, resulting in mismatch of polarization between adjacent antenna elements, thus improving the isolation degree between antenna elements. In order to further improve the isolation degree of the four-element MIMO antenna, a cross-shaped branch is added in the center of the dielectric substrate. The geometric dimensions of the two MIMO antennas are shown in Table 1.

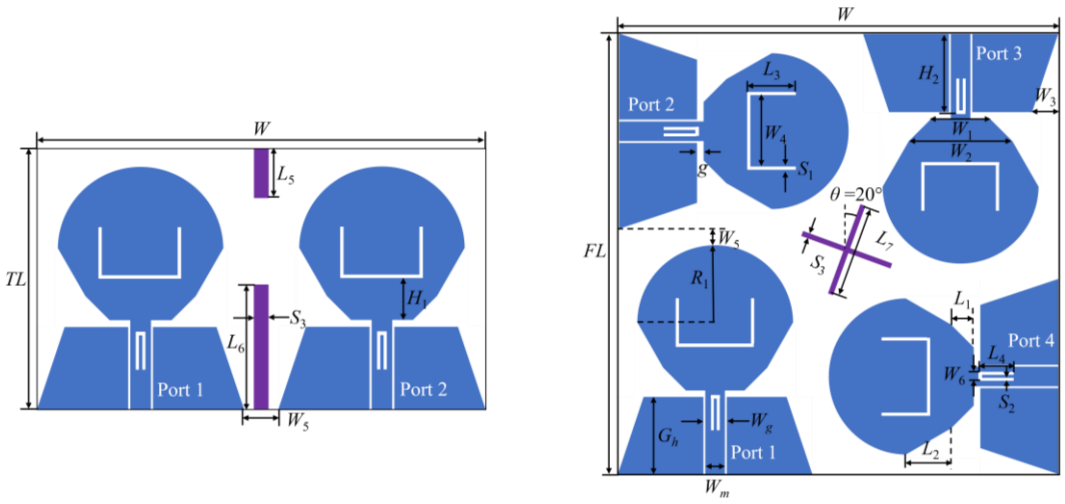

(**a**) (**b**)

Figure 1. Schematic diagram of the UWB MIMO antenna structure: (**a**) Two-element MIMO antenna; (**b**) Four-element MIMO antenna.

Preprints (www.preprints.org) | NOT PEER-REVIEWED | Posted: 12 June 2023 doi:10.20944/preprints202306.0836.v1

Table 1. Antenna geometry (unit: mm).

Parameter	*TL*	*FL*	*W*	*H*	H_1	W_1	W_2	W_3	W_4
Size	38	68	68	1.6	7.6	9	16	4	11.4
Parameter	W_5	W_6	W_7	L_1	L_2	L_3	L_4	L_5	L_6
Size	8	1.4	1.5	3.5	7	7.2	5.2	7	20
Parameter	L_7	S_1	S_2	S_3	S_4	*g*	G_h	R_1	H_2
Size	14	0.3	0.3	2	0.6	1	12	12	11

3. Simulation result analysis

3.1. Notch design and parameter analysis

In order to avoid the interference problem of narrowband communication system, U-shaped slots in the radiation patch of UWB antenna and inverted U-shaped slots in the feeder are used to generate notch properties. In order to verify the mutual independence of the two notch structures, Figure 2 shows the $|S|$-parameter simulation curve corresponding to the UWB MIMO antenna when no notch structures and different number of notch structures are introduced respectively.

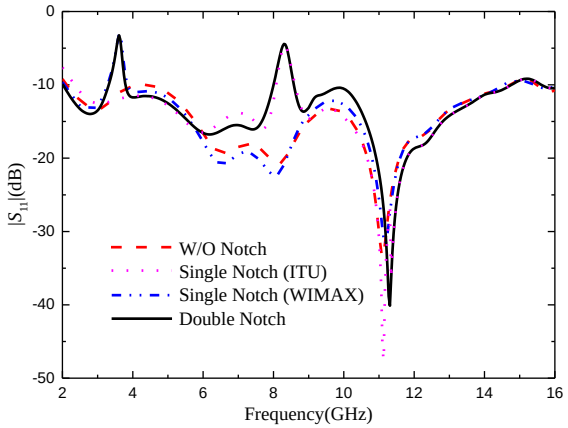

Figure 2. Reflection coefficients of MIMO antenna elements with different numbers of notches.

The non-notch curve in the figure represents the $|S_{11}|$ of the UWB MIMO antenna without notch structure. It can be seen that the working bandwidth of the antenna is 2.12-14.73 GHz, which can cover the UWB band. When only U-shaped slot is loaded, the working bandwidth of the antenna changes to 2.05-14.54 GHz, and the notch appears in the band of 3.28-3.75 GHz, which just covers WIMAX band. When only inverted U-shaped slot is loaded, the working bandwidth changes to 2.25-14.78 GHz, and the notch appears in the band of 8.01-8.61 GHz, which just covers ITU band. When the two slots are etched on the antenna, the working bandwidth changes to 2.02-14.74 GHz, and the notch are generated in the 3.28-3.75 GHz and 7.99-8.58 GHz bands respectively. The range of the notch is almost unchanged compared with the two single notch curves, which proves that the two notch structures have high independence. Finally, accurate filtering of the above two narrow band bands is realized.

In order to study the influence of U-shaped slot and inverted U-shaped slot on the notch characteristics, the key dimensions of the two kinds of notch structures were parameterized and simulated. As shown in Figure 3, when L_3 increases from 6.8 mm to 7.2 mm and other parameters remain unchanged, the center frequency of the notch band 3.28-3.75 GHz changes significantly, decreasing from 3.6 GHz to 3.5 GHz. When L_3=7.0 mm, the stopband bandwidth of the antenna just covers the WIMAX band. Figure 4 shows the influence of the location of the U-shaped slot on antenna. When H_1 increases from 20.4 mm to 20.8 mm, the center frequency of the 3.28-3.75 GHz notch band does not change significantly, but the stopband bandwidth gradually increases. It can be seen from the

Preprints (www.preprints.org) | NOT PEER-REVIEWED | Posted: 12 June 2023 doi:10.20944/preprints202306.0836.v1

above analysis that the notch band can be controlled flexibly by adjusting the length and position of the slot.

Figure 5 shows the $|S_{11}|$ for different values of the key parameter L_4 of the inverted U-shaped slot. As shown in Figure 5, when other parameters remain unchanged and L_4 increases from 4.7 mm to 5.1 mm, the notch band 3.28-3.75 GHz does not change significantly, and the center frequency gradually decreases. By optimizing the key parameters of the two notch structures, it can be seen that the U-shaped slot mainly affects the notch band at 3.28-3.75 GHz, and the inverted U-shaped slot mainly affects the notch band at 7.99-8.58 GHz, with little mutual interference.

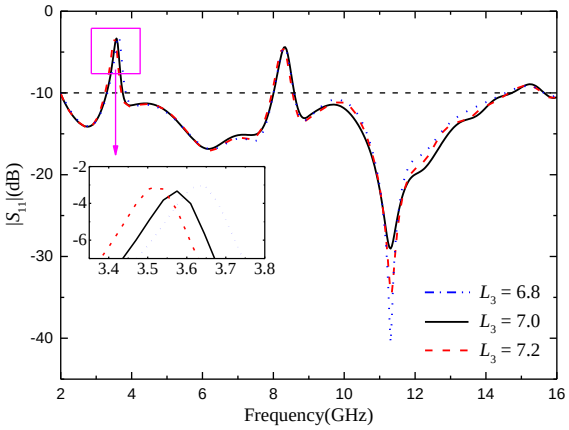

Figure 3. Reflection coefficient of different L_3, the unit of L_3 size (mm).

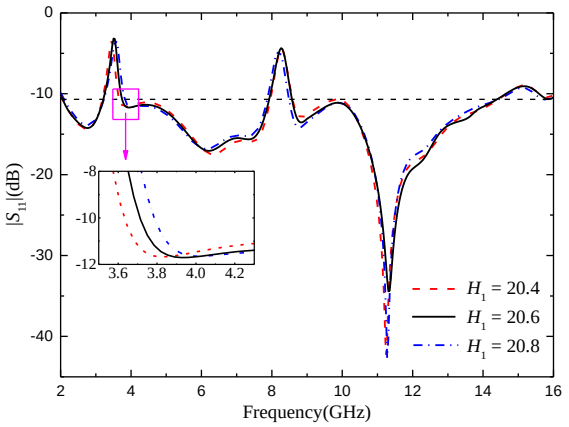

Figure 4. Reflection coefficient of different H_1, the unit of H_1 size (mm).

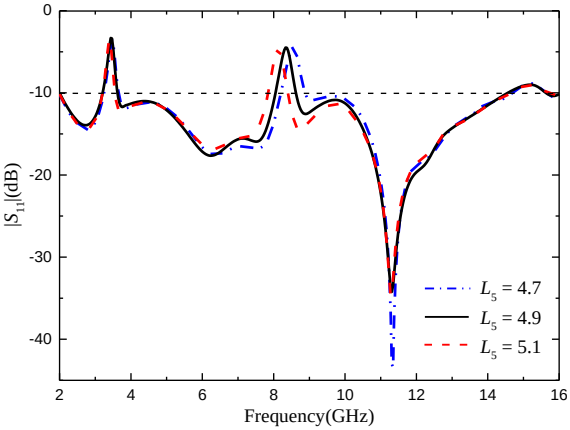

Figure 5. Reflection coefficient of different L_4, the unit of L_4 size (mm).

Preprints (www.preprints.org) | NOT PEER-REVIEWED | Posted: 12 June 2023 doi:10.20944/preprints202306.0836.v1

In order to understand the principle of antenna notch, the antenna was further analyzed. Taking the element antenna as an example, the surface current distribution was simulated and analyzed. Figure 6 shows the antenna surface current distribution at two notch center frequencies of 3.55 and 8.25 GHz and two passband frequency points of 5.5 and 12.5 GHz. It can be seen from the figure that the current at 3.55 GHz is mainly concentrated in the U-shaped slot, and the current at 8.25 GHz is mainly concentrated in the inverted U-shaped slot. Since energy is concentrated in these two places and cannot radiate outward, the notch function is realized. At the passband frequencies of 5.5 GHz and 12.5 GHz, the electric field on the patch and ground plane is evenly distributed, and the electric field near the feeder and the power port is the largest, and the energy can be radiated out, which confirms that the antenna can work normally on the passband frequency.

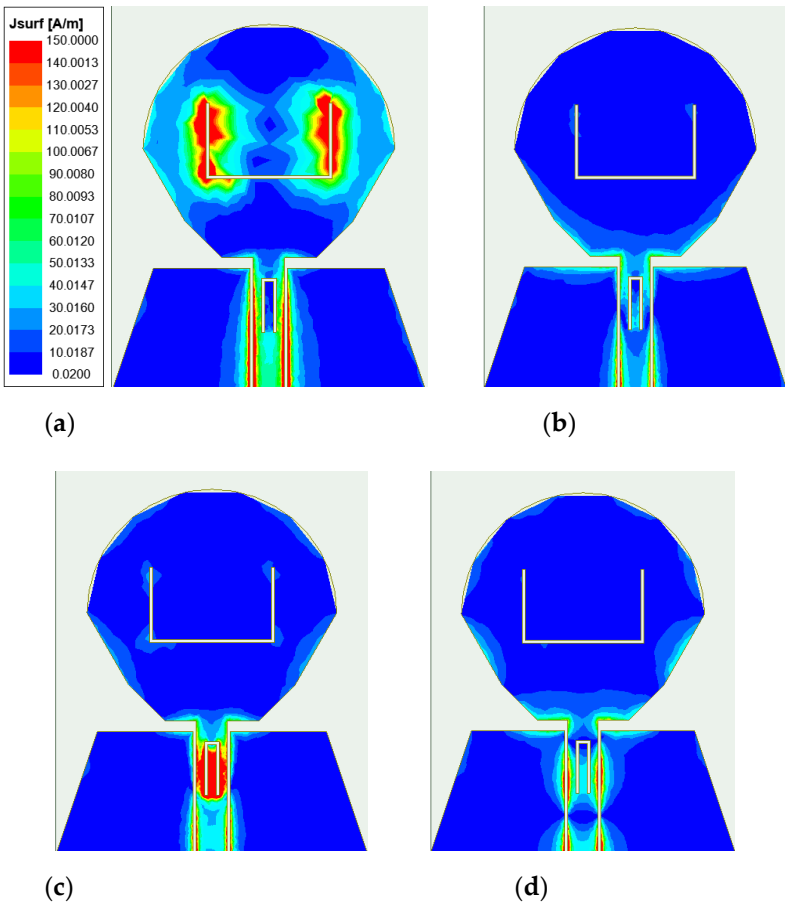

Figure 6. Antenna surface current distribution at four frequency points: (**a**) 3.55 GHz; (**b**) 5.5 GHz; (**c**) 8.25 GHz; (**d**) 12.5 GHz.

3.2. Decoupling design and parameter analysis

3.2.1. Two-element MIMO antenna

In order to study the influence of RB on MIMO antennas and the decoupling effect, two-element MIMO antenna without and with RB are simulated and analyzed, and the parameters of RB are scanned and analyzed.

Figure 7 shows the comparison of $|S|$-parameters before and after antenna loading RB, (a) represents $|S_{11}|$, (b) represents $|S_{21}|$. As can be seen from Figure 7(a), loading RB will deteriorate the antenna's impedance matching in the 4-10 GHz frequency band, but the influence is small and the antenna can still meet the performance indexes of UWB antennas. As can be seen from Figure 7(b), when the RB are not loaded, the antenna's isolation degree is lower than 15 dB in the 8.7-8.9 GHz and 12.64-13.41 GHz bands, and the isolation effect is poor, which does not meet the basic requirements for designing MIMO antennas. However, after loading the RB, the antenna isolation is obviously

Preprints (www.preprints.org) | NOT PEER-REVIEWED | Posted: 12 June 2023 doi:10.20944/preprints202306.0836.v1

improved, especially in the 5-13 GHz frequency band, the antenna isolation is higher than 20 dB, and the antenna isolation is also higher than 17 dB in the other frequency bands of the working frequency band, with an average increase of about 7 dB, indicating an obvious isolation effect. In short, figures (a) and (b) show that RB effectively inhibit electromagnetic coupling between antenna elements, and significantly improve the isolation degree between elements. At the same time, the $|S_{11}|$ of the antenna changed little and remained below -10 dB in the UWB band, and the antenna did not appear impedance mismatch phenomenon.

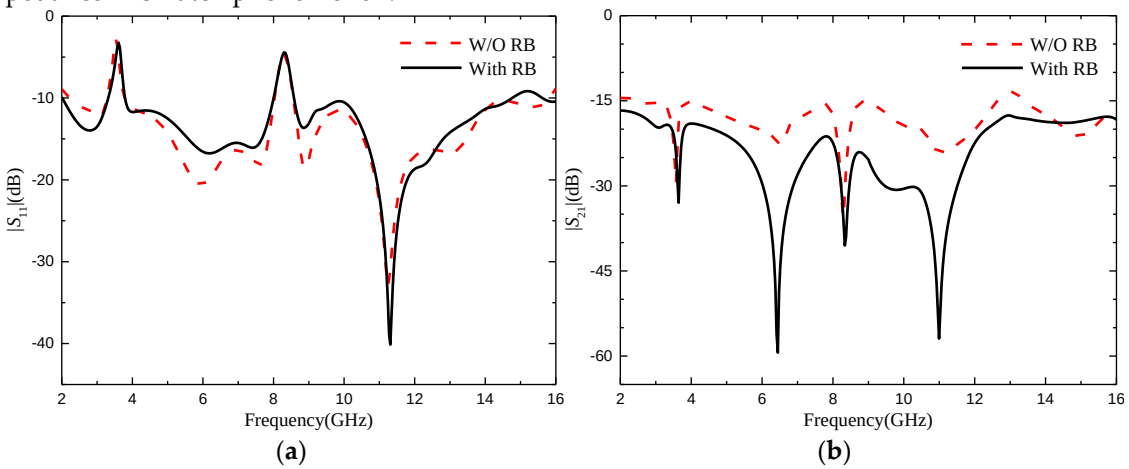

Figure 7. The $|S|$-parameters with or without RB: (**a**) $|S_{11}|$; (**b**) $|S_{21}|$.

In order to further study the influence of isolation structure on antenna performance, the key dimensions of isolation structure are simulated and optimized. Port 1 is set as the excitation port.

Figure 8 represents antenna $|S|$-parameters corresponding to different L_6 values, where (a) represents $|S_{11}|$ and (b) represents $|S_{21}|$. As can be seen from Figure (b), with the increase of L_6, the degree of isolation between the two antenna elements also increases, resulting in better decoupling effect. As can be seen from figure (a), the change of L_6 has little effect on the overall antenna impedance matching, but it has some effect on the range of the notch band. When L_6=20 mm, the notch band just covers the WIMAX band. In summary, when L_6=20 mm, the antenna can not only have high isolation, but also accurately cover the WIMAX band, and its isolation is higher than 15 dB, which meets the basic design requirements of MIMO antenna and has a good decoupling effect.

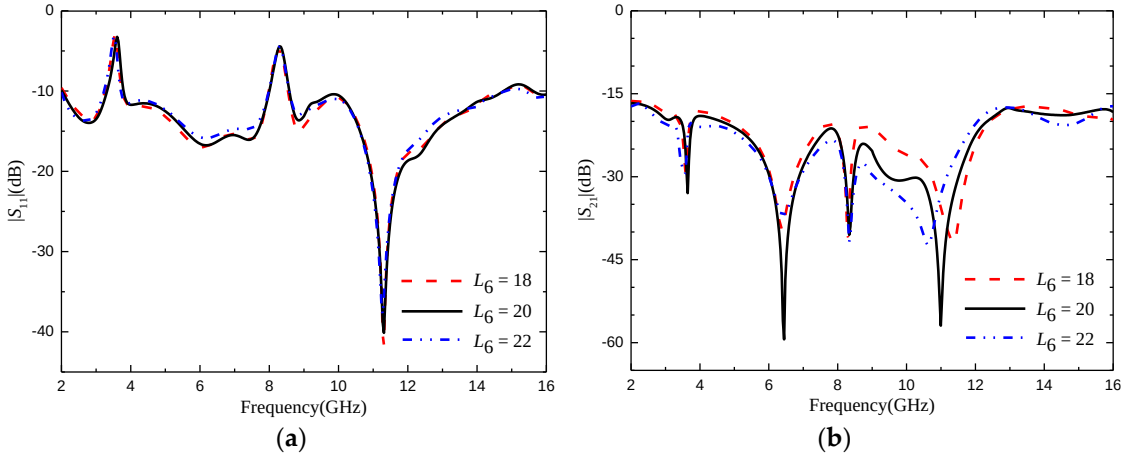

Figure 8. $|S|$-parameters with different L_6, the unit of L_6 size (mm): (**a**) $|S_{11}|$; (**b**) $|S_{21}|$.

Through simulation and optimization, it is found that other dimensions of isolation branches have little influence on antenna impedance matching, and have no significant effect on the improvement of isolation degree, so it will not be analyzed and described.

In order to more directly reflect the function of RB, Figure 9 shows the surface current comparison diagram of without and with RB at frequencies of 3 GHz, 7.25 GHz and 11.6 GHz. It can be clearly

Preprints (www.preprints.org) | NOT PEER-REVIEWED | Posted: 12 June 2023 doi:10.20944/preprints202306.0836.v1

seen from the comparison figure that when the RB is not added, there are more green areas on the feeder and radiation patch of the antenna element where port 2 is located, which indicates that the surface current intensity of the antenna element where port 2 is located is relatively large, and further proves that part of the energy of port 1 is coupled to port 2. When the rectangular decoupling structure was added between the two antenna elements, it could be seen that the surface current intensity of the radiation patch of the antenna element where port 2 was located decreased significantly, which indicated that most of the energy was separated by the RB, and also proved that port 1 had little energy coupled to port 2. The comparison shows that the decoupling structure can well isolate the interference between antenna elements, improve the isolation degree between two ports.

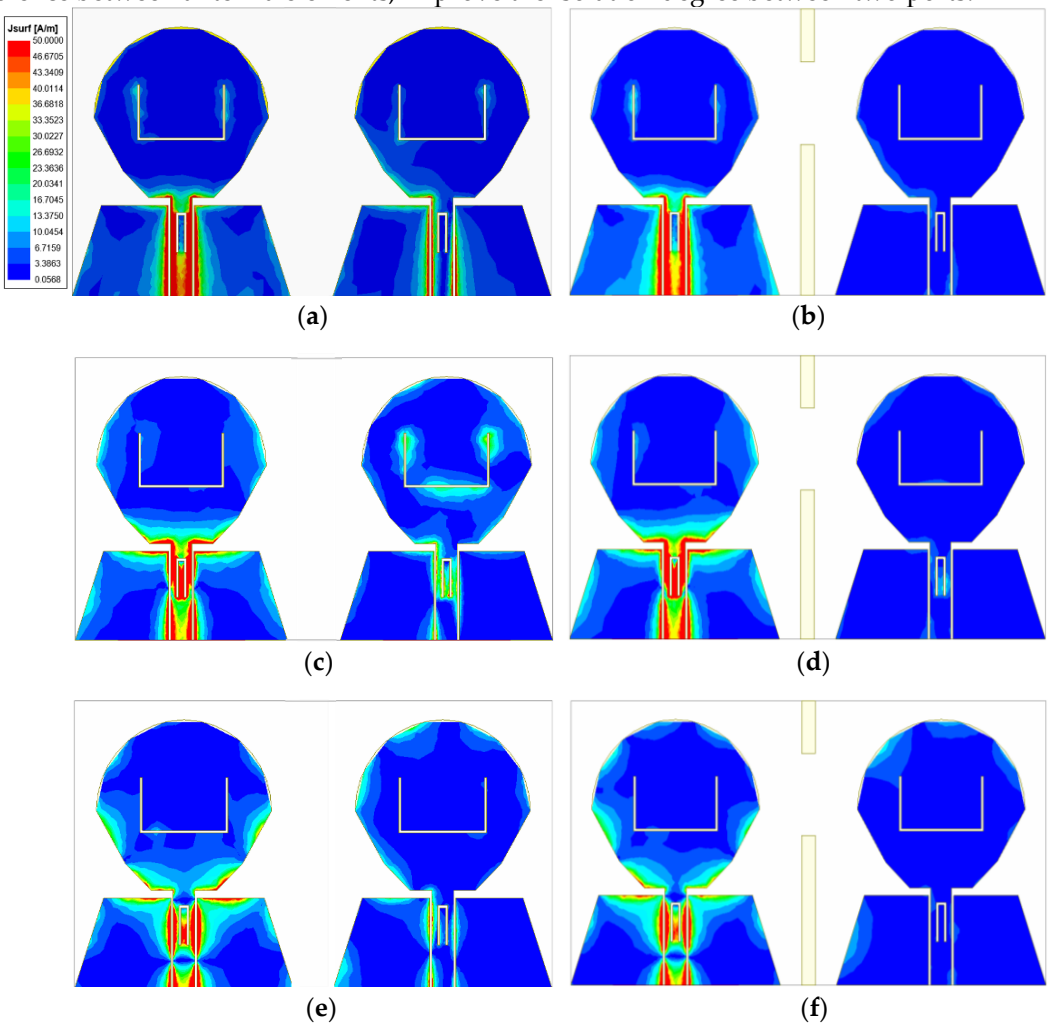

Figure 9. Antenna surface current distribution at: (**a**) 3 GHz without adding RB; (**b**) 3 GHz with adding RB (**c**) 7.25 GHz without adding RB; (**c**) 7.25 GHz with adding RB; (**e**) 11.6 GHz without adding RB; (**e**) 11.6 GHz with adding RB.

3.2.2. Four-element MIMO antenna

After increasing the number of MIMO antenna elements, it will increase the difficulty of decoupling. Therefore, each element of the four-element MIMO antenna is placed orthogonal first. The orthogonal placement of antenna elements will lead to the polarization mismatch of adjacent antennas, thus improving isolation degree between antenna elements. Due to the four-element MIMO antenna has a symmetrical structure, the $|S_{11}|$ of each antenna element is equal, while the isolation degree between antenna elements meet $|S_{ij}| = |S_{ji}|$ ($i \neq j$; i, $j \leq 4$). In order to more convenient to study the variation of the $|S|$-parameters of this MIMO antenna, only the $|S|$-parameters of port 1 can be studied. Figure 10 shows the $|S|$-parameters of the four-element MIMO antenna. It can be seen from the figure that the working bandwidth of the antenna is 2.17-14.71 GHz, in which the notch band of the U-shaped slot is 3.26-3.79 GHz, and the notch band of the inverted U-shaped slot is 7.93-8.51 GHz.

Preprints (www.preprints.org) | NOT PEER-REVIEWED | Posted: 12 June 2023 doi:10.20944/preprints202306.0836.v1

When port 1 is excited, the isolation degree between port 1 and port 2 and between port 1 and port 4 is higher than 23 dB, and the isolation degree between port 1 and port 3 is higher than 15 dB in the working bandwidth. It can be proved that the orthogonal placement of antenna elements can reduce the coupling between antenna elements and obtain good polarization diversity effect. Since the isolation between port 1 and port 3 just meets the basic design requirements, considering that the addition of antenna elements will increase the instability of antenna operation, it is necessary to further improve the isolation between port 1 and port 3.

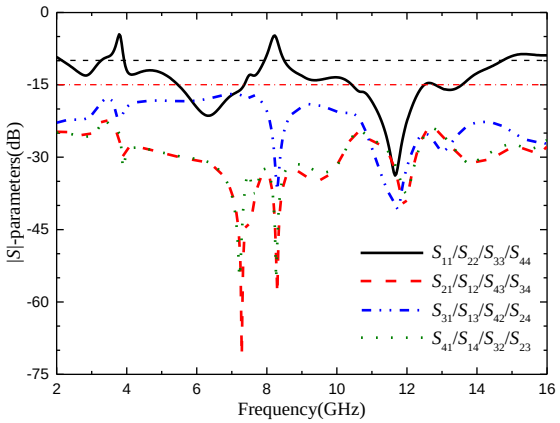

Figure 10. $|S|$-parameters of the four-element MIMO antenna.

In order to further improve the isolation degree between the antenna elements of the four-element MIMO antenna, the center of the dielectric substrate is loaded with cross-shaped branch for decoupling. In order to study the influence of cross-shaped branch on antenna performance, the key parameters of the cross-shaped branch are scanned and optimized. Figure 11 is the $|S|$-parameters of the four-element MIMO antenna after loading the cross-shaped branch. As can be seen from Figure 11, the addition of cross-shaped branch significantly improves the isolation degree between port 1 and port 3, but has little impact between port 1 and other ports. The isolation degree between ports is higher than 21 dB, which has a good decoupling effect. The working bandwidth of the four-element MIMO antenna is 2.13-14.62 GHz, in which the notch band of the U-shaped slot becomes 3.27-3.77 GHz, and the notch band of the inverted U-shaped slot becomes 7.89-8.65 GHz. The two frequency bands can still cover the WIMAX and ITU band respectively. The antenna has accurate notch property and good impedance matching.

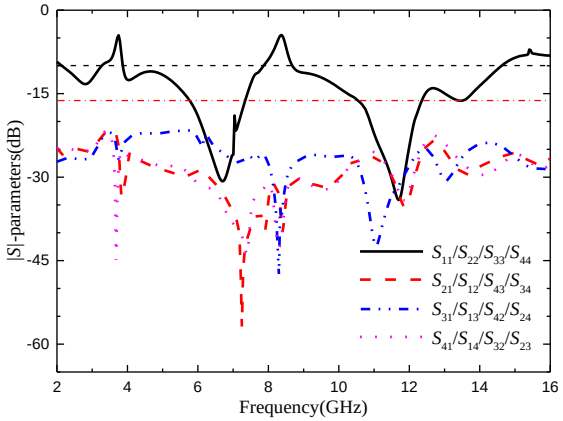

Figure 11. The $|S|$-parameters of the four-element MIMO antenna with the cross branch.

Through simulation analysis, it is found that the rotation angle θ of the cross-shaped branch has a great influence on the notch band of the four-element MIMO antenna, and the length of the cross branch has a significant effect on improving the isolation between port 1 and port 3. The θ was set as 10-30 deg, and the step size was set as 2 deg. Figure 12 shows $|S_{11}|$ with different θ values. It can be

Preprints (www.preprints.org) | NOT PEER-REVIEWED | Posted: 12 June 2023 doi:10.20944/preprints202306.0836.v1

seen from the figure that when θ increases from 10 to 30 deg, the center frequency of the notch band corresponding to U-shaped slot gradually increases, while that corresponding to the notch band corresponding to the inverted U-shaped slot gradually decreases. When θ=20 deg, the two notch bands exactly cover the WIMAX and ITU band. The L_7 is set from 10 to 16 mm, and the step is set to 1 mm. $|S_{31}|$ corresponding to different values of L_7 is shown in Figure 13. As can be seen from the figure, as L_7 increases, the isolation between port 1 and port 3 gradually increases. However, with the change of the value of L_7, the accuracy of the notch band will be slightly affected. When L_7=13 mm, the antenna has a high isolation degree and the notch band can achieve accurate coverage.

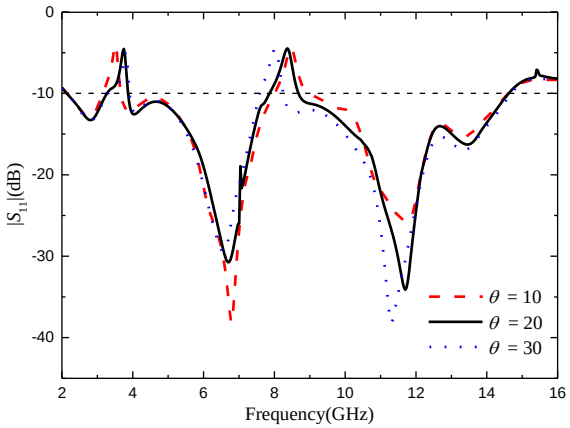

Figure 12. $|S_{11}|$ with different θ, the unit of θ size (degree).

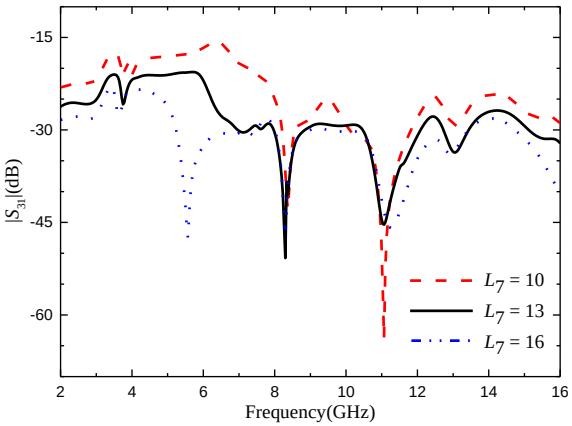

Figure 13. $|S_{31}|$ with different L_7, the unit of L_7 size (mm).

In order to more directly reflect the effect of orthogonal placement of antenna elements and the isolation effect after loading the cross-shaped branch, Figure 14 shows the surface current comparison diagram of the four-element MIMO antenna at the frequencies of 4.5 GHz, 7.25 GHz and 11.6 GHz. As can be seen from Figure 14, when the cross-shaped branch is not loaded, part of the energy of port 1 is coupled to other ports. From the current distribution on the antenna surface, the coupled energy is small, which proves that the isolation degree can be improved by placing antenna elements orthogonal to each other. By observing the current distribution of the antenna surface with the cross-shaped branch loaded, it is found that the energy coupled from port 1 to other ports is less than that without the cross-shaped branch loaded. The currents on both sides of the cross-shaped branch form opposite directions, and the electric fields radiated by the cross-shaped branch cancel each other in opposite directions to realize the decoupling effect, which further proves that the cross-shaped branch can improve the isolation between antenna elements.

Preprints (www.preprints.org) | NOT PEER-REVIEWED | Posted: 12 June 2023 doi:10.20944/preprints202306.0836.v1

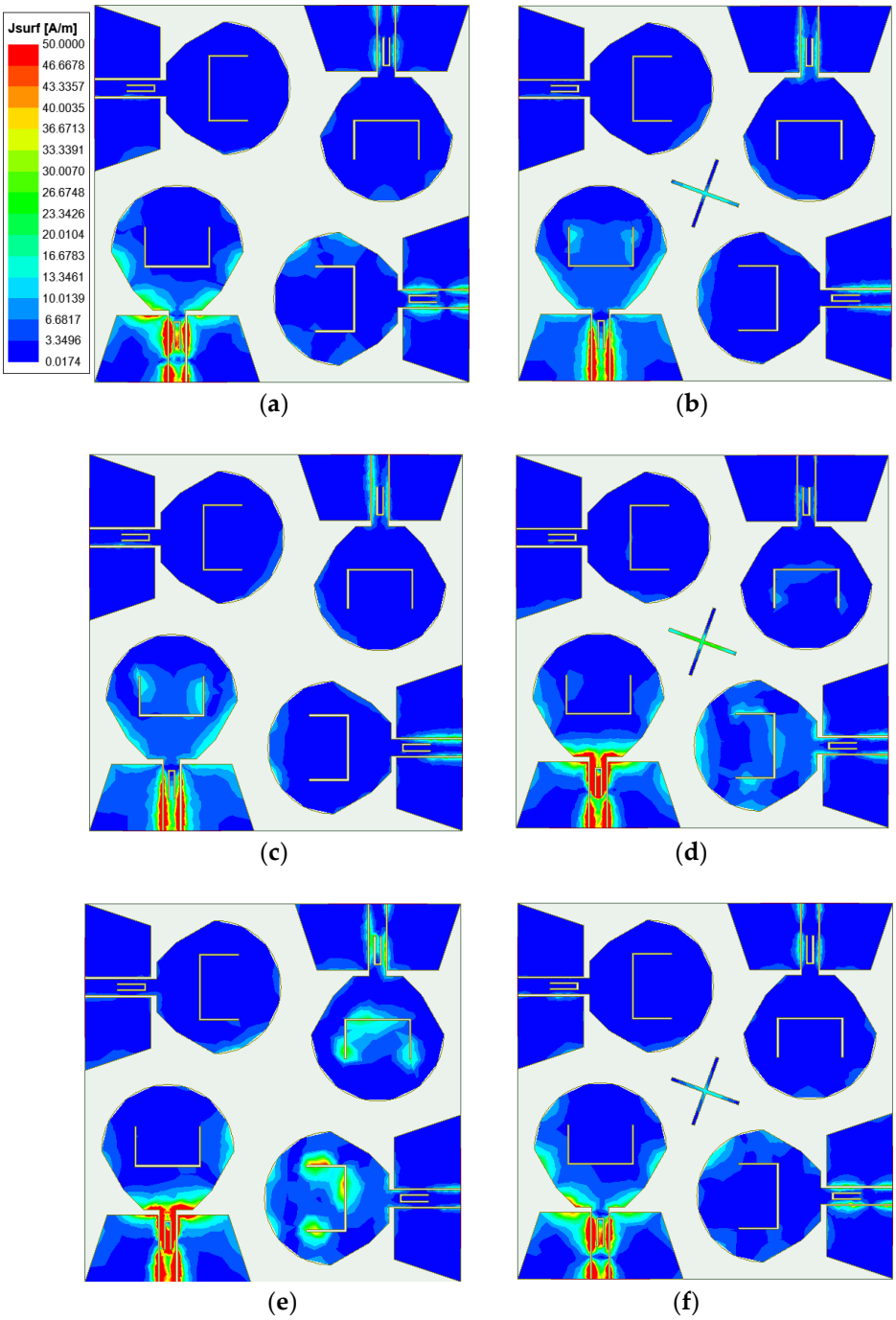

Figure 14. Antenna surface current distribution at: (**a**) 4.5 GHz without adding cross-shaped branch; (**b**) 4.5 GHz with adding cross-shaped branch; (**c**) 7.25 GHz without adding cross-shaped branch; (**d**) 7.25 GHz with adding cross-shaped branch; (**e**) 11.6 GHz without adding cross-shaped branch; (**e**) 11.6 GHz with adding cross-shaped branch.

4. Measured results and analysis

In order to verify the performance of the two MIMO antennas designed, the antennas are manufactured according to the data in Table 1. Both MIMO antennas are fed by coplanar waveguide (CPW) and printed on F4BTM440 dielectric substrates with a relative dielectric constant of 4.4 and a tangent loss of 0.0015. Vector network analyzer (N5244A) and microwave anechoic chamber were used to measure the MIMO antenna $|S|$-parameter and far-field radiation pattern, as shown in Figure 15 and 16.

Preprints (www.preprints.org) | NOT PEER-REVIEWED | Posted: 12 June 2023 doi:10.20944/preprints202306.0836.v1

(**a**) (**b**)

Figure 15. Photographs of the measured $|S|$-parameter scenarios using vector network analyzer Keysight N5244A: (**a**) Two-element MIMO antenna; (**b**) Four-element MIMO antenna.

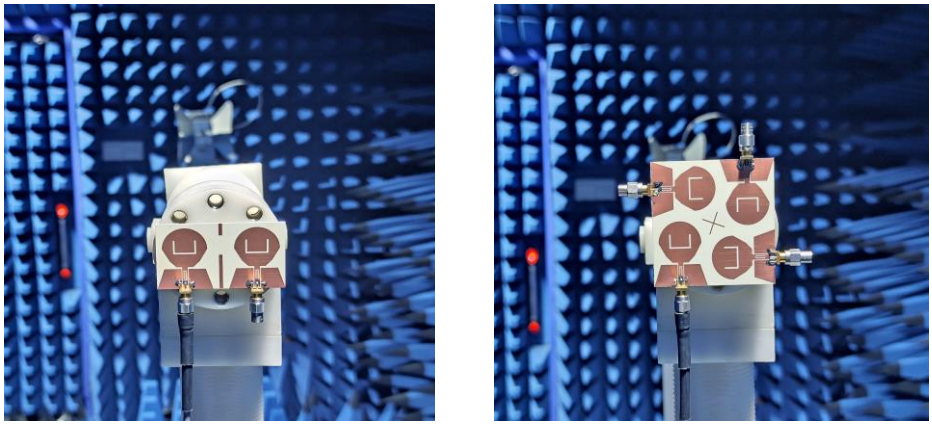

(**a**) (**b**)

Figure 16. Photographs of far-field radiation pattern measurements using a microwave anechoic chamber, (**a**) Two-element MIMO antenna; (**b**) Four-element MIMO antenna.

4.1. S-parameter

4.1.1. Two-element MIMO antenna

Figure 17 shows the two-element UWB MIMO antenna simulation and the measured $|S|$-parameters, due to the symmetry of the antenna unit, only consider the $|S|$-parameters of port 1. As can be seen from the figure, the measured working bandwidth of the antenna is 2.45-14.88 GHz, which can cover the UWB band. The notch band corresponding to the U-shaped slot is 3.26-3.75 GHz, and the notch band corresponding to the inverted U-shaped slot is 7.96-8.65 GHz, which can cover the WIMAX and ITU band respectively. The measured isolation between two antenna ports is higher than 18 dB. By comparing the simulation results and the measured results in Figure 17, it can be seen that the measured $|S|$-parameters are roughly consistent with the simulated $|S|$-parameters. However, due to the errors caused by antenna machining, welding process and network analysis instruments, the measured and simulated values have a small difference.

4.1.2. Four-element MIMO antenna

Figure 18 shows the simulation and the measured $|S|$-parameters of the four-element UWB MIMO antenna, due to the symmetry of the antenna element, only consider the $|S|$-parameters of port 1. As can be seen from the figure, the measured working bandwidth of the antenna is 2.14-14.95 GHz, which can cover the UWB band. The notch band corresponding to the U-shaped slot is 3.02-3.99 GHz,

Preprints (www.preprints.org) | NOT PEER-REVIEWED | Posted: 12 June 2023 doi:10.20944/preprints202306.0836.v1

and the notch band corresponding to the inverted U-shaped slot is 7.56-8.58 GHz. The bandwidth of the two notch bands becomes wider. However, WIMAX and ITU band can still be covered separately. The measured isolation degree between each antenna port is higher than 20 dB, which proves that the isolation degree between antenna elements is high and they can maintain independent normal operation. By comparing the simulation results and the measured results in Figure 18, it can be seen that the measured $|S|$-parameters are roughly consistent with the simulated $|S|$-parameters, which proves that the antenna has good performance.

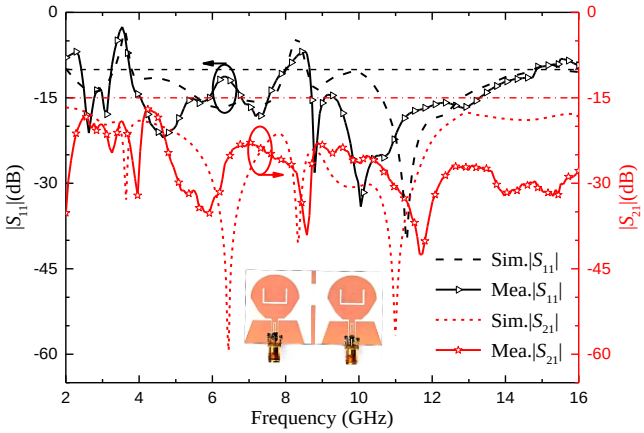

Figure 17. Simulation and measured $|S|$-parameters of the proposed two-element MIMO antenna.

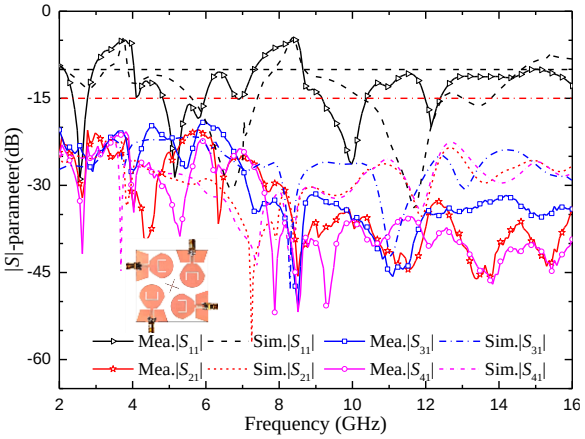

Figure 18. Simulation and measured $|S|$-parameters of the proposed four-element MIMO antenna.

4.2. Radiation pattern

4.2.1. Two-element MIMO antenna

Figure 19 shows the measured radiation pattern of the two-element MIMO antenna at the operating frequencies of 4.2, 6.8 and 10.6 GHz when port 1 is excited and port 2 is connected to a 50 Ω load. It can be seen from the figure that the radiation pattern of E-plane is good at 4.2 GHz and 6.8 GHz, but becomes irregular at 10.6 GHz, while the H-plane shows omnidirectional characteristics at 4.2 GHz and 6.8 GHz, and becomes irregular at 10.6 GHz. With the increase of frequency, the wavelength of the antenna decreases and is no longer much larger than the size of the antenna. The antenna no longer has the characteristics of an electrically small antenna. Therefore, the radiation pattern of the antenna changes and no longer presents the radiation pattern similar to that of a monopole antenna. Although the shape degradation and deformation of antenna radiation pattern will occur at high frequency, the radiation intensity still meets the communication requirements of UWB antenna. It can be seen from the radiation pattern of the antenna that the antenna is an omnidirectional antenna, which is suitable for most scenarios of UWB technology application.

Preprints (www.preprints.org) | NOT PEER-REVIEWED | Posted: 12 June 2023 doi:10.20944/preprints202306.0836.v1

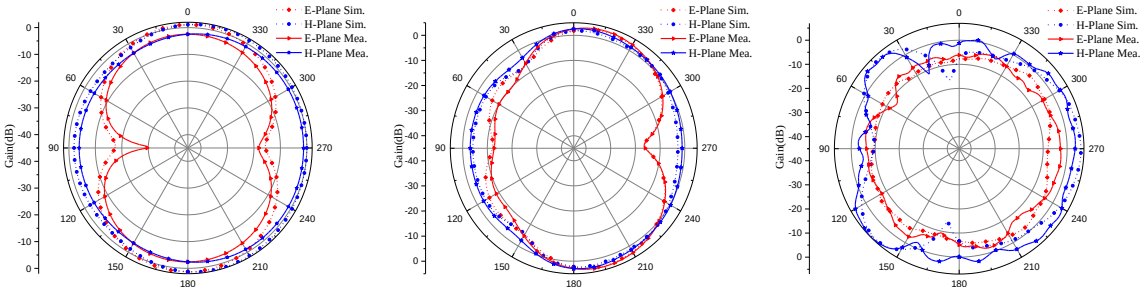

Figure 19. The measured radiation pattern of the proposed two-element MIMO antenna: (**a**) 4.2 GHz; (**b**) 6.8 GHz; (**c**) 10.6 GHz.

4.2.2. Four-element MIMO antenna

Figure 20 shows the measured radiation pattern of the four-element MIMO antenna at the operating frequencies of 4.0, 7.6 and 11.6 GHz when port 1 is excited and other ports are connected to a 50 Ω load. It can be seen from the figure that the radiation pattern of E-plane is good at 4.0 GHz and 7.6 GHz, but becomes irregular at 11.6 GHz, while the H-plane shows omnidirectional characteristics at 4.0 GHz and 7.6 GHz, and becomes irregular at 11.6 GHz. Although the antenna radiation pattern is deformed at high frequency, it still meets the design requirements of UWB antenna. The antenna is omnidirectional and suitable for most UWB technology application scenarios.

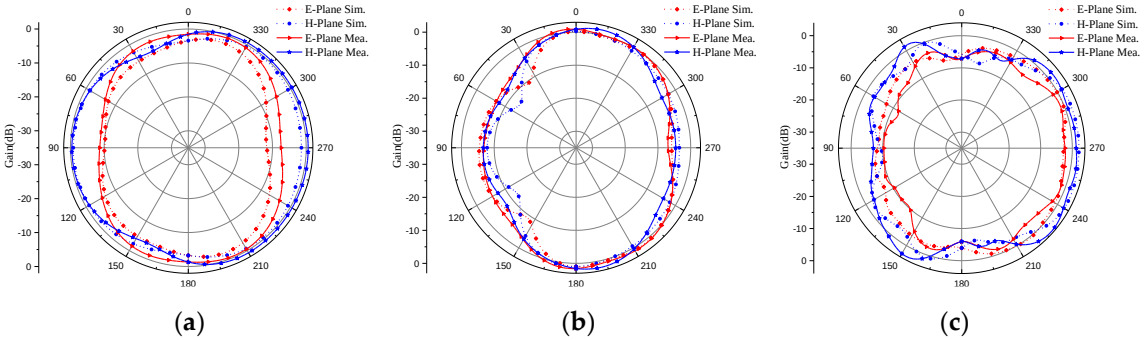

Figure 20. The measured radiation pattern of the proposed four-element MIMO antenna: (**a**) 4.0 GHz; (**b**) 7.6 GHz; (**c**) 11.6 GHz.

4.3. Envelope Correlation Coefficient

The envelope correlation coefficient is used to measure the correlation between the channels of MIMO antenna units. It refers to the correlation between different signal amplitudes received by the antenna. For MIMO antennas, smaller ECC means weaker channel correlation and better system performance. In general engineering applications, if the ECC is less than 0.5 [24], it can be considered that the antenna channels can work independently. The calculation of S parameter for ECC [23]is shown in Formula (3):

$$\rho_{eij} = \frac{|S_{ii}^{*}S_{ij} + S_{ji}^{*}S_{jj}|^2}{(1-|S_{ii}|^2 - |S_{ji}|^2)(1-|S_{jj}|^2 - |S_{ij}|^2)} \quad (3)$$

Figure 21(a) shows the ECC of the two proposed MIMO antennas, which shows that the ECC is very small (< 0.02) in the whole passband bandwidth except for the notch band. Although the ECC is affected by these notch structures, it is less than 0.03 in the whole impedance bandwidth. Similarly, it can be seen from Figure 21(b) that except for the notch band, the ECC within the passband bandwidth is less than 0.02, and the entire impedance bandwidth is less than 0.05. The ECC values of the two proposed MIMO antennas are low and meet the standard of ECC less than 0.5, which indicates that

Preprints (www.preprints.org) | NOT PEER-REVIEWED | Posted: 12 June 2023 doi:10.20944/preprints202306.0836.v1

the antennas have good diversity performance and can be effectively applied in multi-antenna systems.

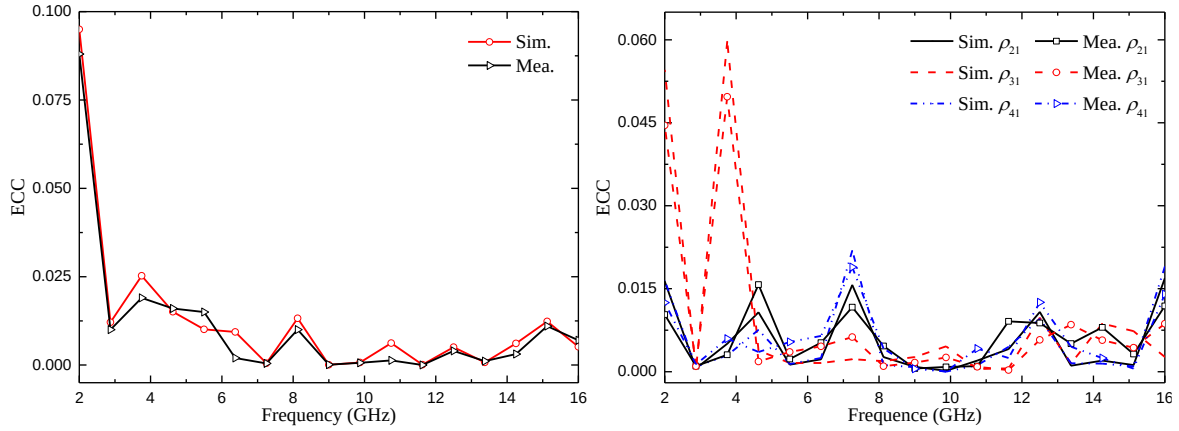

Figure 21. ECC of the proposed antenna: (**a**) Two-element MIMO antenna; (**b**) Four-element MIMO antenna.

4.4. Diversity Gain

Diversity gain (DG) is another important parameter to measure the performance of MIMO antenna [23]. The ideal value is 10 dB. It can be calculated as [4]:

$$DG = 10\sqrt{1-|ECC_{ij}|^2} \tag{4}$$

The measured and simulated DG of the proposed two MIMO antennas are shown in Figure 22. From Figure 22, we can confirm that the diversity gain of the two MIMO antennas is very close to 10 dB, and the maximum value is 9.999dB. We also noticed that the value of the diversity gain was very similar for the simulated and measured cases.

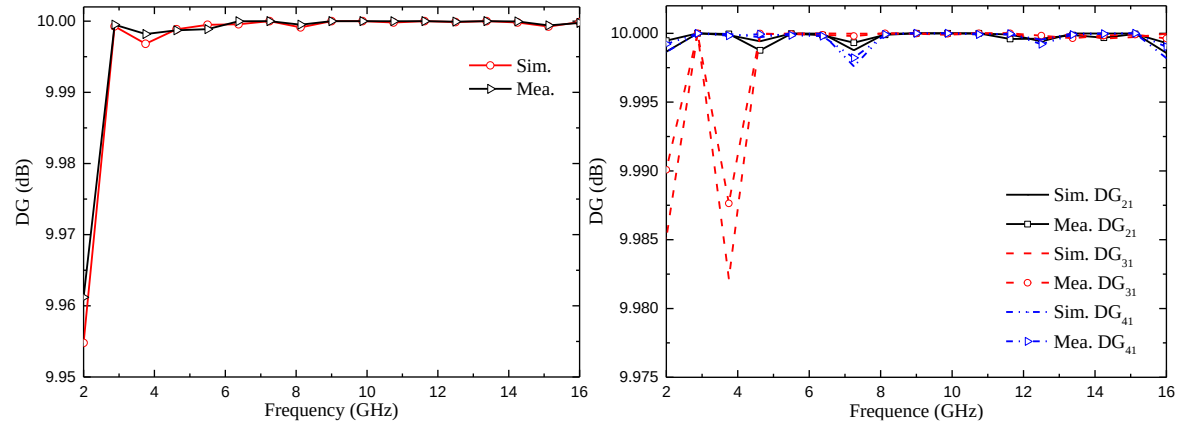

Figure 22. DG of the proposed antenna: (**a**) Two-element MIMO antenna; (**b**) Four-element MIMO antenna.

4.5. Radiation efficiency

As an energy conversion device, antenna converts high-frequency current energy into electromagnetic wave energy or electromagnetic wave energy into high-frequency current energy. However, due to various losses in the transmission process, such as antenna dielectric loss, copper loss and component loss, the input antenna power can only be partially converted into electromagnetic wave energy. The efficiency of the antenna is used to characterize the degree of such conversion. The calculation method is shown in Formula (5):

Preprints (www.preprints.org) | NOT PEER-REVIEWED | Posted: 12 June 2023 doi:10.20944/preprints202306.0836.v1

$$\eta = \frac{P_r}{P_{in}} = \frac{P_r}{P_r + P_d} \tag{5}$$

Where P_{in} is the power entering the antenna, P_r is the radiated power of the antenna, and P_d is the lost power of the antenna.

The radiation efficiency of the two proposed MIMO antennas is shown in Figure 23. It can be seen from the figure that, except for the notch band, the minimum radiation efficiency of the two MIMO antennas is also higher than 80% in the whole passband bandwidth range, which proves that the antennas achieve good radiation energy conversion and fully meet the requirements of wireless devices. However, the radiation efficiency of the antenna decreases obviously in the two notch bands, which further proves that the energy radiation of the antenna in the notch band can be reduced by notch design.

In order to further verify the effectiveness of this design, the experimental results of the designed antenna are compared with those of the references. The comparative experimental results antenna impedance bandwidth, relative impedance bandwidth, number of MIMO antenna units, notch band, isolation, peak gain and ECC. The details for each comparison item are shown in Table 2. In the references listed in Table 2, most antennas are not designed for notch and have low peak gain. The radiation efficiency of the antenna in [16, 20] are also relatively low and the antenna in [14] has low isolation and narrow impedance bandwidth. By comparing the data in Table 2, it can be found that the designed antenna has a wide impedance bandwidth, with relative impedance bandwidth higher than 140%, low ECC and good radiation efficiency. In a word, the antenna performance is better.

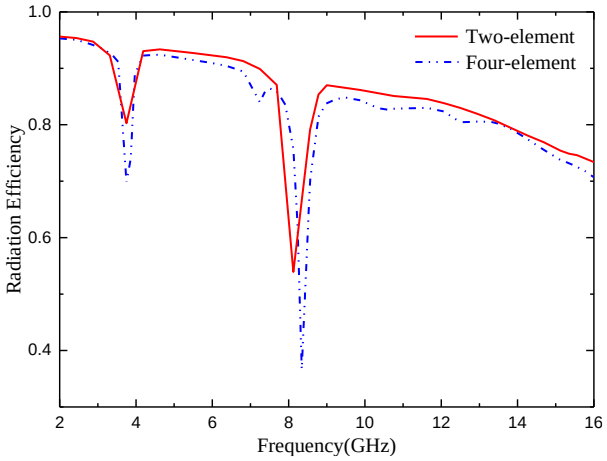

Figure 23. Radiation efficiency of the proposed antenna for 2- and 4- element antennas.

Preprints (www.preprints.org) | NOT PEER-REVIEWED | Posted: 12 June 2023 doi:10.20944/preprints202306.0836.v1

Table 2. Comparison of antennas in references and this paper

Ref.	Impedance bandwidth (GHz)	Relative bandwidth (%)	Number of elements	Notch band	Isolation (dB)	ECC	Gain (dB)	Radiation efficiency (%)
[12]	4.3-15.63	114	2	-	20	<0.0075	<5.35	>85
[14]	2.9-12	122	2	-	15	<0.02	<4.2	>60
[16]	2.9-12.2	123	2	-	17.8	-	<3.8	-
[17]	2.1-20	161	4	WI-MAX	25	<0.02	<5.8	>80
[19]	3.2-12	115	4	-	22	<0.5	<4	>80
[20]	4.5-16.4	114	4	-	20	<0.002	<7.8	>61
This work	**2.45-14.88**	**143**	**2**	**WI-MAX /ITU**	**>17**	**<0.02**	**<5.7**	**>82**
	2.14-14.95	**150**	**4**	**WI-MAX /ITU**	**>20**	**<0.02**	**<5.9**	**>80**

5. Conclusions

Two compact UWB-MIMO antennas with high isolation have been checked. One is a two-element MIMO antenna located parallel with an impedance bandwidth from 2.45-14.88 GHz, which is loaded with two RB to achieve an isolation higher than 17 dB in the passband range. The other is a four-element MIMO antenna located at quadrature with an impedance bandwidth from 2.14-14.95 GHz. By placing the antenna elements orthogonal and loading the cross branches, the antenna has an isolation degree of more than 20 dB in the passband range. Both can suppress the interference of WIMAX and ITU bands to UWB communication, which are with simple in structure and easy to process. At the same time, they have stable gain and very lower ECC, which can be widely used in UWB communication system.

Author Contributions: Design and concept, L.W., Z.W.L.; methodology, Z.W.L. and L.W.; experiment, L.W.; resources, L.W.; writing-original draft preparation, Z.W.L. and L.W.; writing-review and editing, H.X.Z.; validation, H.X.Z.; supervision, H.X.Z.; project administration, H.X.Z.

Funding: This research received no external funding.

Data Availability Statement: Not applicable.

Acknowledgments: This work is supported by the National Natural Science Foundation of China, under Grants 62071166.

Conflicts of Interest: The authors declare no conflict of interest.

References

1. Mescia, L.; Mevoli, G.; Lamacchia, C.M.; Gallo, M.; Bia, P.; Gaetano, D.; Manna, A. sinuous antenna for UWB radar applications. Sensors **2022**, 22, 248. https://doi.org/10.3390/s22010248
2. Wang, M.; Tian, X.W.; Song, L.Z. A ultra wideband dual-polarized antenna with high isolation degree for passive radar application, *Electromagnetics* **2021**, *41*, 409-419. https://doi.org/10.1080/02726343.2021.1989753
3. Mohammad, K.; Sajad, M.A. Radar cross-section reduction of an UWB MIMO antenna using image theory and its equivalent circuit model. *Int. J. RF Microw. Comput. Aided Eng.* **2021**, *31*, 22563. https://doi.org/10.1002/mmce.22563

4. Emadian, S.R.; Ahmadi-Shokouh, J.; Ghobadi, C.; Nourinia, J. Study on frequency and impulse response of novel triple band notched UWB antenna in indoor environments. *AEU-Int. J. Electron. Commun*. **2018**, *96*, 93-106. https://doi.org/10.1016/j.aeue.2018.09.003.
5. Martínez-Lozano, A.; Blanco-Angulo, C.; García-Martínez, H.; Gutiérrez-Mazón, R.; Torregrosa-Penalva, G.; Ávila-Navarro, E.; Sabater-Navarro, J.M. UWB-Printed rectangular-based monopole antenna for biological tissue analysis. *Electronics* **2021**, *10*, 304. https://doi.org/10.3390/electronics10030304
6. Kissi, C.; Särestöniemi, M. Receiving UWB antenna for wireless capsule endoscopy communications. *Prog. Electromagn. Res. C* **2020**, *101*, 53-69.
7. Zhong, Z.P.; Liang, J.J.; Fan, M.L.; Huang, G.L.; He, W.; Chen, X.C.; Yuan, T. A compact CPW-fed UWB antenna with quadruple rejected bands. *Microw. Opt. Technol. Lett.* **2019**, *61*, 2795–2800. https://doi.org/10.1002/mop.31976
8. Iqbal, A.; Smida, A.; Mallat, N.K.; Islam, M.T.; Kim, S. A Compact UWB Antenna with Independently Controllable Notch Bands. *Sensors* **2019**, *19*, 1411. https://doi.org/10.3390/s19061411
9. Liu, J.B.; Ding, W.H.; Chen, J.H.; Zhang, A. New ultra-wideband filter with sharp notched band using defected ground structure. *Prog. Electromagn. Res. Lett.* **2019**, *83*, 99–105. http://dx.doi.org/10.2528/PIERL18111302
10. Siddiqui, J.Y.; Saha, C.; Sarkar, C.; Shaik, L.A.; Antar, Y. Ultra-wideband antipodal tapered slot antenna with integrated frequency-notch characteristics. *IEEE Trans. Antennas Propag.* **2018**, *66*, 1534–1539. https://doi.org/10.1109/TAP.2018.2790176
11. Luo, S.; Chen, Y.; Wang, D.; Liao, Y.; Li, Y. A monopole UWB antenna with sextuple band-notched based on SRRs and U-shaped parasitic strips. *AEU-Int. J. Electron. Commun.* **2020**, *120*, 153206. https://doi.org/10.1016/j.aeue.2020.153206
12. Mu, W.; Lin, H.; Wang, Z.; Li, C.; Yang, M.; Nie, W.; Wu, J. A flower-shaped miniaturized UWB-MIMO antenna with high isolation. *Electronics* **2022**, *11*, 2190. https://doi.org/10.3390/electronics11142190
13. Wang, L.L.; Du, Z.H.; Yang, H.L.; Ma, R.Y.; Zhao, Y.C.; Cui, X.Q.; Xi, X.L. Compact UWB MIMO antenna with high isolation using fence-type decoupling structure. *IEEE Antennas Wirel. Propag. Lett.* **2019**, *18*, 1641–1645. https://doi.org/10.1109/LAWP.2019.2925857
14. Ren, J.; Hu, W.; Yin, Y. Compact printed MIMO antenna for UWB applications. *IEEE Antennas Wirel. Propag. Lett.* **2014**, *13*, 1517-1520. https://doi.org/10.1109/LAWP.2014.2343454.
15. Zhang, S.; Pedersen, G.F. Mutual coupling reduction for UWB MIMO antennas with a wideband neutralization line. *IEEE Antennas Wirel. Propag. Lett.* **2016**, *15*, 166▪169. https://doi.org/10.1109/LAWP.2015.2435992
16. Boumaaza, K.; Hebib, S.; Mouffok, L. Compact two-port tapered microstrip feed MIMO antenna for UWB applications. 2022 2nd International Conference on Advanced Electrical Engineering (ICAEE), Constantine, Algeria, 2022; pp. 1-4. https://doi.org/10.1109/ICAEE53772. 2022.9962060
17. Rekha, V.S.D.; Pardhasaradhi, P.; Madhav, B.T.P.; Devi, Y.U. Dual band notched orthogonal 4-element MIMO antenna with isolation for UWB applications. *IEEE Access* **2020**, *8*, 145871–145880. https://doi.org/10.1109/ACCESS.2020.3015020
18. Agarwal, S.; Rafique, U.; Ullah, R.; Ullah, S.; Khan, S.; Donelli, M. Double overt-leaf shaped CPW-Fed four port UWB MIMO antenna. *Electronics* **2021**, *10*, 3140. https://doi.org/10.3390/electronics10243140
19. Srivastava, G.; Mohan, A. Compact MIMO slot antenna for UWB applications. *IEEE Antennas Wirel. Propag. Lett.* **2016**, *15*, 1057-1060. https://doi.org/10.1109/LAWP.2015.2491968
20. Kumar, P.; Pathan, S.; Vincent, S.; Kumar, O.P.; N, Y.; Kumar, P.; Shetty, P.R.; Ali, T. A compact quad-port UWB MIMO antenna with improved isolation using a novel mesh-like decoupling structure and unique DGS. *IEEE T. Circuits-II.* **2023**, *70*, 949-953. https://doi.org/10.1109/TCSII.2022.3220542.
21. Arumugam, S.; Manoharan, S.; Palaniswamy, S.K.; Kumar, S. Design and Performance Analysis of a Compact Quad-Element UWB MIMO Antenna for Automotive Communications. *Electronics* **2021**, *10*, 2184. https://doi.org/10.3390/electronics10182184
22. Kolangiammal, S.; Balaji, L.; Mahdal, M. Design of compact planar monopole UWB MIMO antenna with four orthogonal elements and tapered fed configuration for wireless diversity applications. *Electronics* **2022**, *11*, 3087. https://doi.org/10.3390/electronics11193087
23. He, Z.; Jin, J. Compact quad-port MIMO antenna with ultra-wideband and high isolation. *Electronics* **2022**, *11*, 3408. https://doi.org/10.3390/electronics11203408
24. Zhao, X.; Riaz, S.; Geng, S. A reconfigurable MIMO/UWB MIMO antenna for cognitive radio applications. *IEEE Access* **2019**, *7*, 46739-46747. https://doi.org/10.1109/ACCESS.2019.2909810